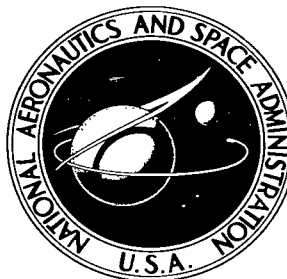


NASA TECHNICAL NOTE



NASA TN D-3700

*e.1*

NASA TN D-3700



TECH LIBRARY KAFB, NM

TRANSONIC AERODYNAMIC  
INVESTIGATION OF TENSION SHELL  
AND BLUNTED 100° CONICAL SHAPES  
FOR UNMANNED ENTRY VEHICLES

*by Charles D. Harris*

*Langley Research Center*

*Langley Station, Hampton, Va.*





TRANSONIC AERODYNAMIC INVESTIGATION  
OF TENSION SHELL AND BLUNTED  $100^\circ$  CONICAL SHAPES  
FOR UNMANNED ENTRY VEHICLES

By Charles D. Harris

Langley Research Center  
Langley Station, Hampton, Va.

NATIONAL AERONAUTICS AND SPACE ADMINISTRATION

---

For sale by the Clearinghouse for Federal Scientific and Technical Information  
Springfield, Virginia 22151 - Price \$2.00

TRANSONIC AERODYNAMIC INVESTIGATION  
OF TENSION SHELL AND BLUNTED 100° CONICAL SHAPES  
FOR UNMANNED ENTRY VEHICLES

By Charles D. Harris  
Langley Research Center

SUMMARY

An experimental investigation of a spherically blunted 100° cone and two tension shell configurations with varying nose-bluntness ratios for use in unmanned entry into low-density planetary atmospheres has been conducted by the National Aeronautics and Space Administration at Mach numbers from 0.30 to 1.20 and at angles of attack from approximately 0° to 40°.

The results show that the models were longitudinally stable, with centers of pressure located rearward of the base at all test conditions. The tension shell configurations exhibited substantially higher axial-force coefficients than the 100° cone although the variation of axial-force coefficient with Mach number at zero angle of attack was similar for all configurations. An increase in tension shell body length resulted in a reduction of the axial-force coefficients and a more forward center-of-pressure location. Variation in nose bluntness had no significant effect on the longitudinal aerodynamic characteristics of the tension shell configurations.

INTRODUCTION

Analytical studies (refs. 1 and 2) and experimental investigations (refs. 3 to 5) by the National Aeronautics and Space Administration have indicated that the payload capability of vehicles designed for entry into low-density planetary atmospheres may be improved by using configurations which carry the primary structural loading in tension. Such tension shell configurations show considerable promise for achieving low structural weight and high drag.

This report presents the results of an investigation made to assess experimentally some of the transonic aerodynamic characteristics of shapes defined by this tension shell concept and also of a spherically blunted 100° conical body. The conical body not only provides a competitive high-drag shape for comparison but also adds to the available data for spherically blunted large-angle cones in the transonic Mach number range. The

investigation was conducted in the Langley 8-foot transonic pressure tunnel at Mach numbers from 0.30 to 1.20 and at angles of attack from about  $0^\circ$  to  $40^\circ$ .

## SYMBOLS

The aerodynamic force and moment data are referred to the body axes as indicated in figure 1, and the origin of the body axes for the various configurations is shown in figure 2. Model force and moment coefficients are based on the model base diameter and area.

$A^2$	tension shell shape parameter from reference 2
$C_A$	axial-force coefficient, $\frac{\text{Axial force}}{qS}$
$C_{A,b}$	axial-force coefficient at model base, $\frac{\text{Axial force at model base}}{qS}$
$C_m$	pitching-moment coefficient, $\frac{\text{Pitching moment}}{qSd}$
$C_{m_\alpha}$	slope of pitching-moment curve, $\frac{\partial C_m}{\partial \alpha}$ , per degree
$C_N$	normal-force coefficient, $\frac{\text{Normal force}}{qS}$
$C_{N_\alpha}$	slope of normal-force curve, $\frac{\partial C_N}{\partial \alpha}$ , per degree
$d$	base diameter, 25.40 centimeters (10.00 in.)
$M$	free-stream Mach number
$q$	free-stream dynamic pressure
$R$	Reynolds number based on $d$
$r$	radial coordinate
$r_b$	base radius
$r_n$	nose radius
$S$	base area, $\pi d^2/4$

x	longitudinal coordinate
$x_{cp}$	longitudinal distance of center of pressure from model base, positive direction forward
$x_{ref}$	longitudinal distance of moment reference center from model base, positive direction forward
$\alpha$	angle of attack, degrees

## APPARATUS AND TEST CONDITIONS

### Models

Model coordinates are given in table I, body geometry is illustrated in figure 2, and photographs of the models are shown in figure 3. The tension shell shapes were derived from structural concepts based on pressure distributions of Newtonian aerodynamics to yield either zero or tension stresses. As discussed in reference 2, the local surface slope of these cusped or flared tension shell bodies may be expressed in terms of the local radial coordinate, the base radius, and a shape parameter  $A^2$  which is associated with the Newtonian pressure distribution and which may be varied to generate a family of shapes. The effect on tension shell model geometry of an increase in the shape parameter  $A^2$  (compare figs. 2(b) and 2(c)) is an increase in body length and a reduction in surface concavity on the cusped or flared portion of the model. In the present investigation, values of  $A^2 = 1.27$  and  $A^2 = 1.40$  were considered. The tension shell with  $A^2 = 1.40$  was 16 percent longer than the tension shell with  $A^2 = 1.27$  for nose-bluntness ratios (nose radius/base radius) of zero. The investigation also included interchangeable tension shell nose caps with nose-bluntness ratios of 0, 0.05, and 0.10.

### Support System

In order to cover the complete angle-of-attack range of this investigation, an adjustable angle-of-attack adapter as shown in figure 2(d) was used. For angles of attack from approximately  $0^\circ$  to  $20^\circ$ , the adjustable adapter was positioned at an angle of  $0^\circ$  relative to the conventional sting; for angles of attack from about  $20^\circ$  to  $40^\circ$ , the adjustable adapter was positioned  $19.8^\circ$  relative to the conventional sting. This support system kept the model near the center line of the tunnel at all angles of attack. A three-component internal strain-gage balance was attached to the forward end of the adjustable adapter and was partially housed within the model. The model balance assembly was shielded from the airstream by means of a shroud which extended approximately 0.34 base diameter from the base of the model.

## Test Conditions

The three models were investigated at Mach numbers from 0.30 to 1.20 and at angles of attack from approximately  $0^\circ$  to  $40^\circ$ . Stagnation temperature was held constant at approximately  $322^\circ\text{ K}$  ( $120^\circ\text{ F}$ ). All tests were conducted at a stream stagnation pressure of 1 atmosphere which resulted in Reynolds numbers, based on model base diameter, from  $1.50 \times 10^6$  at a Mach number of 0.30 to  $3.52 \times 10^6$  at a Mach number of 1.20. Figure 4 gives the variation of Reynolds number and dynamic pressure with Mach number. No attempt was made to fix transition on the models.

## CORRECTIONS AND ACCURACY

The aerodynamic force and moment data presented herein are considered to be free of tunnel boundary interference. The axial-force coefficients have not been adjusted for base pressure effects, but representative base axial-force coefficients are presented.

Examination of the data indicates that discontinuities in the force and moment coefficients occur at an angle of attack of about  $20^\circ$ , which is the angle of attack at which changes in the model support system were made (see fig. 2(d)). The influence of the model support system on the model characteristics apparently varies depending on the relative position of the model and support system. No attempt has been made to correct the data for support-system interference except to the extent of the partial correction inherent in the base axial-force coefficients.

The angles of attack, corrected for deflection of the balance and support system under aerodynamic load, are estimated to be accurate within  $\pm 0.1^\circ$ , and the free-stream Mach number is estimated to be accurate within  $\pm 0.005$ . Balance error, based on 0.5 percent of the maximum design load of each component, is estimated to be within the following limits:

	For M = 0.30	For M = 1.20
$C_N$ . . . . .	$\pm 0.051$	$\pm 0.007$
$C_A$ . . . . .	$\pm 0.051$	$\pm 0.007$
$C_m$ . . . . .	$\pm 0.011$	$\pm 0.002$

## PRESENTATION OF RESULTS

Static longitudinal aerodynamic characteristics of the  $100^\circ$  cone and the tension shell configurations with a nose-bluntness ratio of 0.10 are presented in figure 5. The effect of variations in nose bluntness on the static longitudinal aerodynamic characteristics of the tension shell configurations with shape parameters  $A^2 = 1.27$  and  $A^2 = 1.40$  is shown in figures 6 and 7, respectively. Representative base axial-force coefficients

are presented in figure 8. The effects of variations in Mach number on the pitching-moment and normal-force slopes for an angle of attack of approximately  $4^\circ$  and on the axial-force coefficient at zero angle of attack are presented in figure 9. The pitching-moment and normal-force slopes were obtained from the faired curves in figure 5. Representative center-of-pressure locations, measured from the base, are presented in figure 10 for an angle of attack of about  $4^\circ$  and were obtained from the following equation:

$$\frac{x_{cp}}{d} = \frac{C_{m,\alpha=4^\circ} - C_{m,C_N=0}}{C_{N,\alpha=4^\circ}} + \frac{x_{ref}}{d}$$

In this equation,  $C_{m,\alpha=4^\circ}$  and  $C_{N,\alpha=4^\circ}$  are the values at an angle of attack of  $4^\circ$  of  $C_m$  and  $C_N$ , respectively, and  $C_{m,C_N=0}$  is the value of  $C_m$  when  $C_N = 0$ .

## DISCUSSION

Comparison of the basic longitudinal aerodynamic data for the  $100^\circ$  cone and the tension shell configurations presented in figure 5 and summarized in figure 9 indicates a reduction in the pitching-moment and normal-force slopes and an increase in axial-force coefficient for the tension shell configurations. These results may be associated with the increased local compression on the concave surface of the tension shells. Both the  $100^\circ$  cone and the tension shell configurations were longitudinally stable at all test conditions, however, and variation of axial-force coefficients with Mach number at zero angle of attack (fig. 9) was similar for all configurations.

In figure 10 the variation of representative center-of-pressure locations with Mach number is shown for an angle of attack of approximately  $4^\circ$ . This figure indicates that the centers of pressure are located rearward of the base under all conditions and in general move farther rearward with increasing subsonic Mach number. A small forward movement is noted as the free-stream Mach number becomes supersonic.

The increase in body length and the attendant decrease in surface concavity as the tension shell shape parameter  $A^2$  is increased from 1.27 to 1.40 afford a lower axial-force coefficient (figs. 5 and 9) and a more forward center-of-pressure location (fig. 10). These variations in aerodynamic characteristics with shape parameter are associated with the compression characteristics of the flow over the concave portion of the body.

The basic data shown in figures 6 and 7 and the summary data presented in figure 10 show that the variation in the nose bluntness employed in the present investigation had no significant effects on the static longitudinal aerodynamic characteristics of the tension shell configurations.

## CONCLUDING REMARKS

An experimental investigation of several shapes for use in unmanned entry into low-density planetary atmospheres has been conducted in the Langley 8-foot transonic pressure tunnel at Mach numbers from 0.30 to 1.20 and at angles of attack from approximately  $0^\circ$  to  $40^\circ$ . The results include the longitudinal aerodynamic characteristics of a spherically blunted  $100^\circ$  cone and two tension shell configurations with varying nose-bluntness ratios. From these results the following conclusions were reached:

1. The models were longitudinally stable, with the centers of pressure located rearward of the base at all test conditions.
2. The tension shell configurations exhibited substantially higher axial-force coefficients than the  $100^\circ$  cone although the variation of axial-force coefficients with Mach number at zero angle of attack was similar for all configurations.
3. Increasing the length of the tension shell configuration resulted in a reduction of the axial-force coefficients and a forward movement of the center of pressure.
4. Variation in nose bluntness had no significant effect on the longitudinal aerodynamic characteristics of the tension shell configurations.

Langley Research Center,  
National Aeronautics and Space Administration,  
Langley Station, Hampton, Va., July 18, 1966,  
124-08-06-07-23.

## REFERENCES

1. Guy, L. D.: Tension Shell Structures for Low Density Entry Vehicles. Presented at AIAA Second Annual Meeting and Technical Display (San Francisco, Calif.), July 1965.
2. Anderson, Melvin S.; Robinson, James C.; Bush, Harold G.; and Fralich, Robert W.: A Tension Shell Structure for Application to Entry Vehicles. NASA TN D-2675, 1965.
3. Bernot, Peter T.: Longitudinal Stability Characteristics of Several Proposed Planetary Entry Vehicles at Mach 6.73. NASA TN D-2785, 1965.
4. Robinson, James C.; and Jordan, Alfred W.: Exploratory Experimental Aerodynamic Investigation of Tension Shell Shapes at Mach 7. NASA TN D-2994, 1965.
5. Deveikis, William D.; and Sawyer, James Wayne: Aerodynamic Characteristics of Tension Shell Shapes at Mach 3.0. NASA TN D-3633, 1966.

TABLE I. - COORDINATES OF TENSION SHELL MODELS

$r/r_b$	$x/r_b$ for -	
	Tension shell with $A^2 = 1.27$	Tension shell with $A^2 = 1.40$
0	1.000	1.160
.05	.919	1.065
.10	.839	.995
.15	.760	.877
.20	.683	.787
.25	.608	.699
.30	.536	.615
.35	.467	.534
.40	.402	.459
.45	.341	.388
.50	.284	.322
.55	.232	.262
.60	.185	.209
.65	.143	.160
.70	.106	.118
.75	.076	.083
.80	.048	.053
.85	.027	.030
.90	.012	.014
.95	.004	.003
1.00	0	0

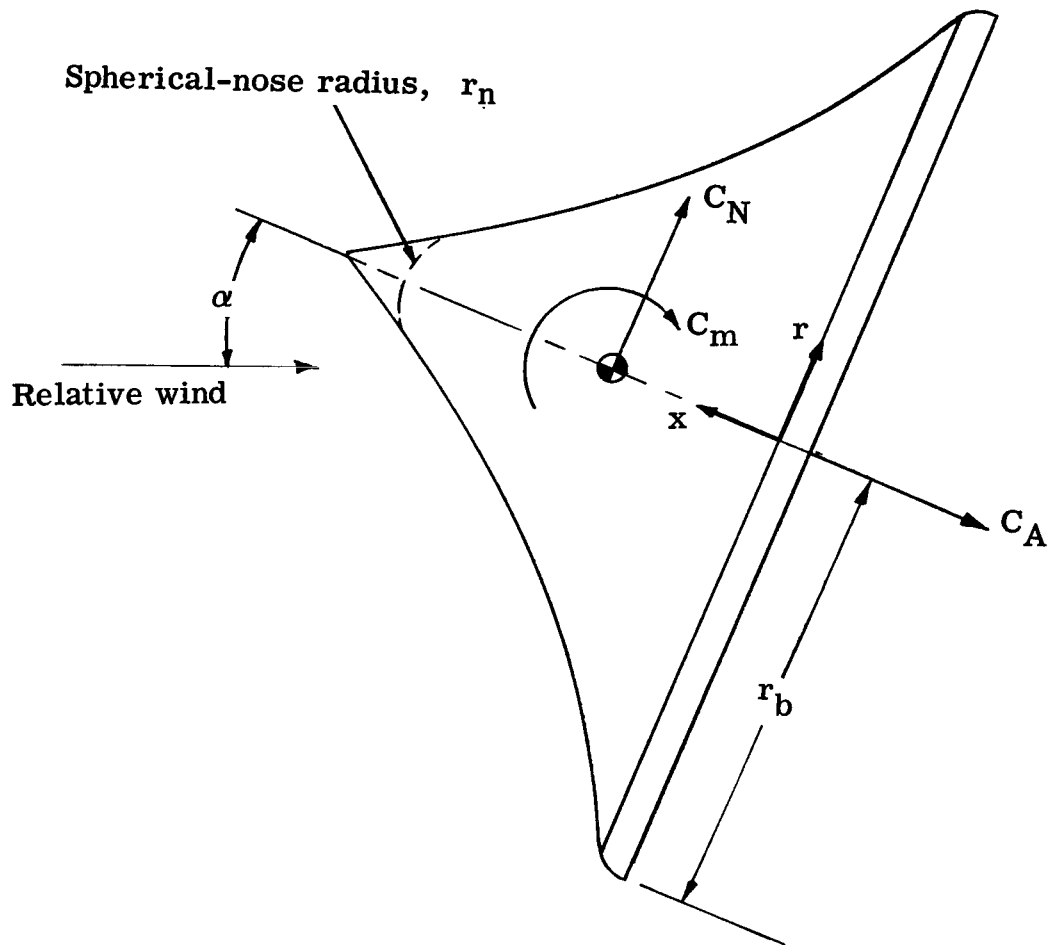
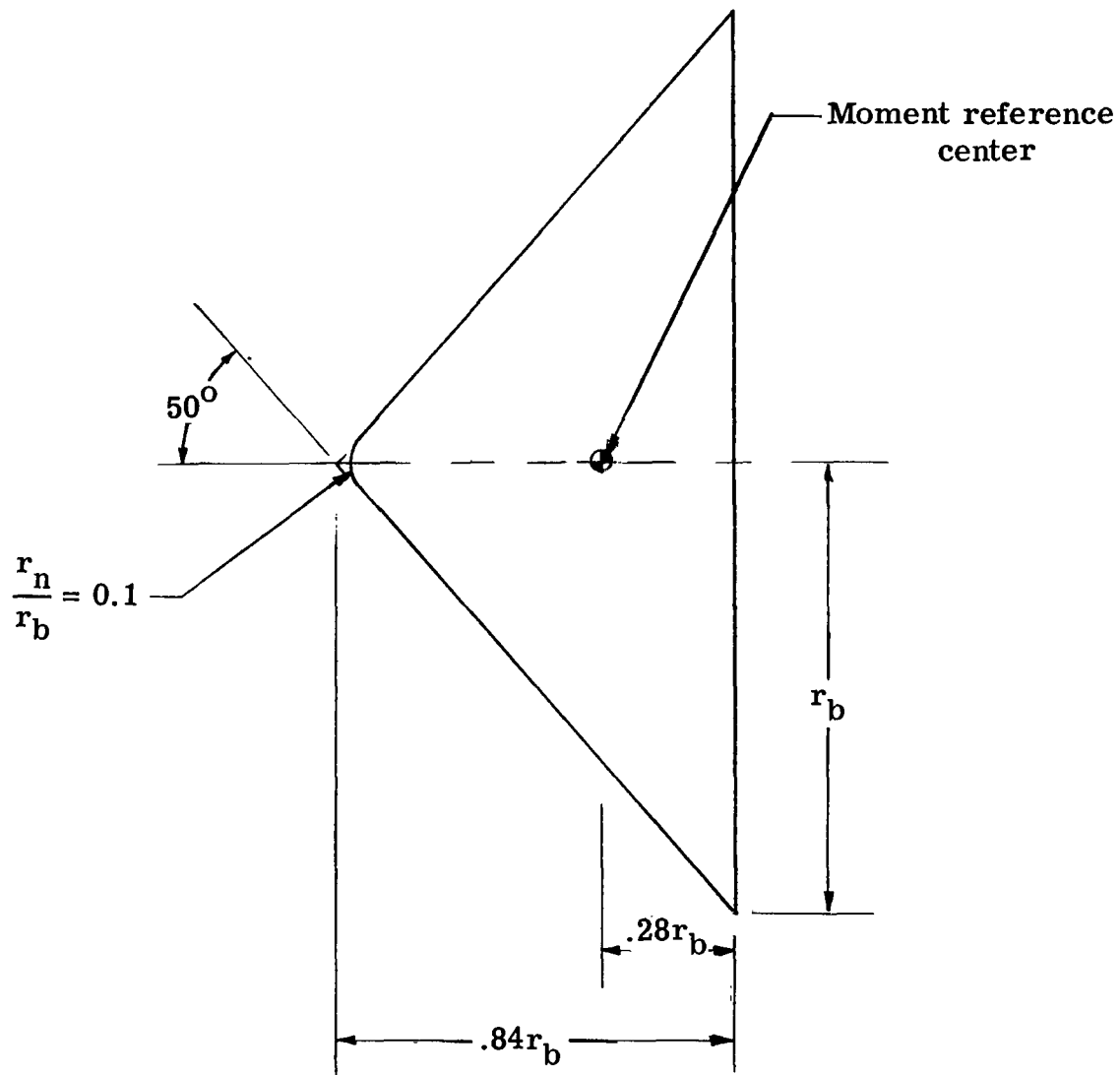
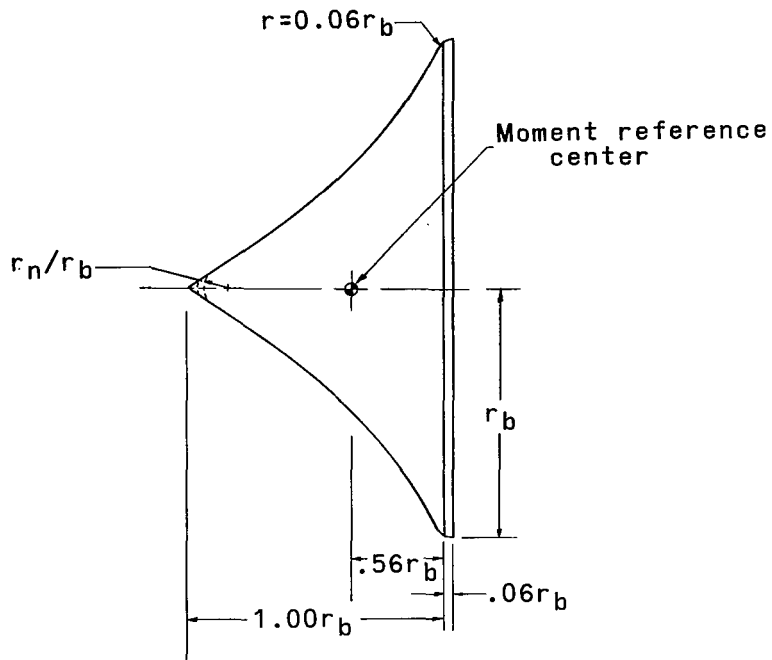


Figure 1.- Sketch indicating the orientation of model axes and force reference axes.

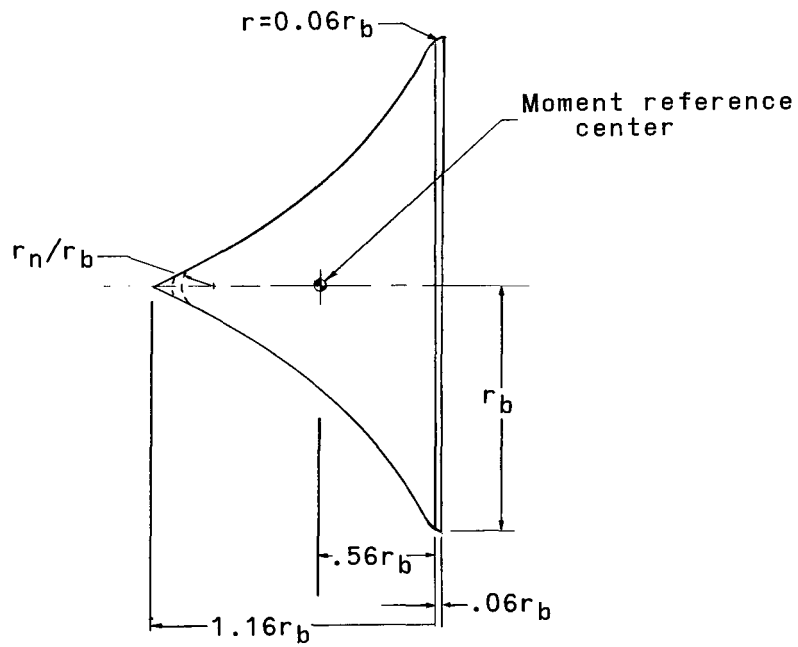


(a)  $100^\circ$  conical body.

Figure 2.- Drawings of low-density entry models.  $r_b = 12.70$  cm (5.00 in.).

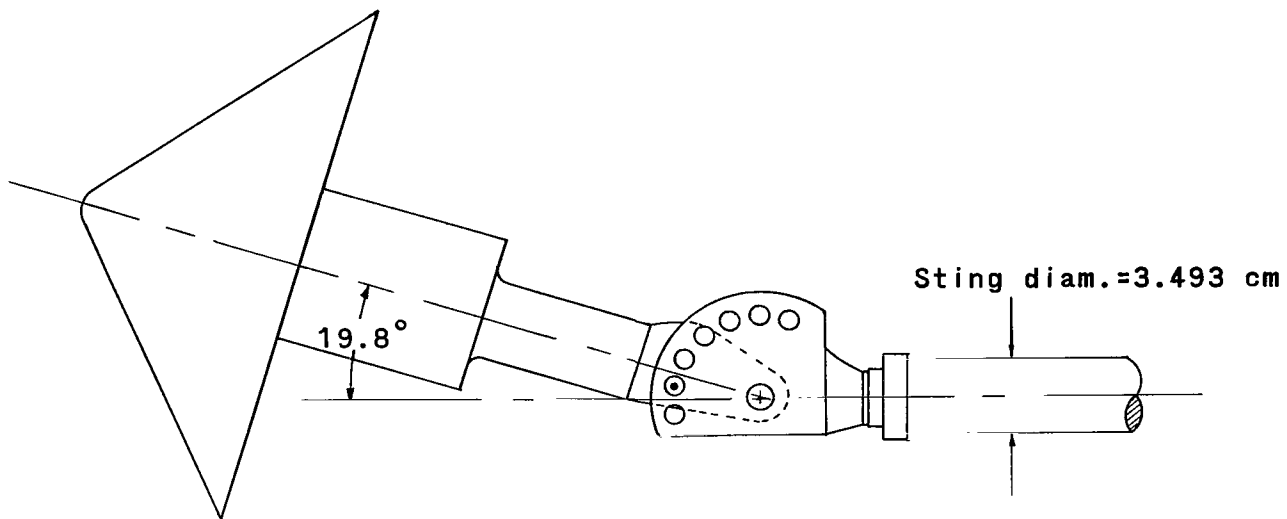


(b) Tension shell with  $A^2 = 1.27$ .

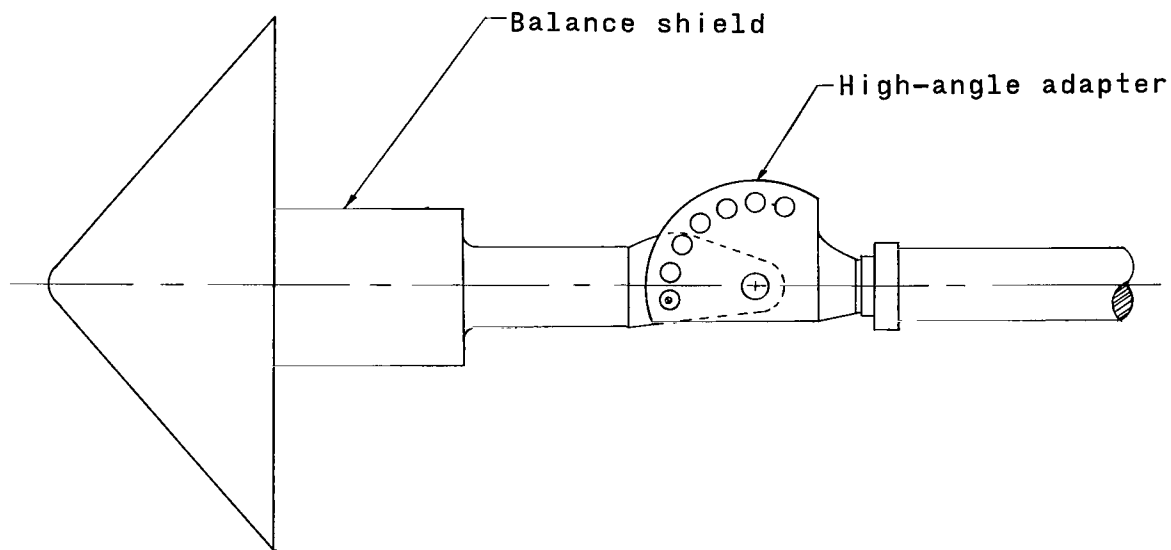


(c) Tension shell with  $A^2 = 1.40$ .

Figure 2.- Continued.



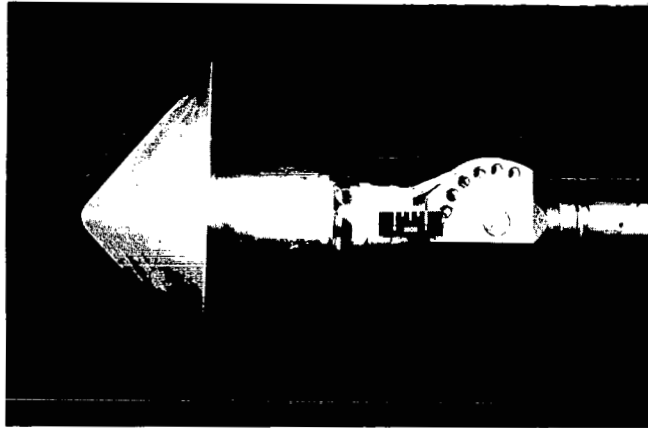
Adapter position for angle-of-attack range from 20° to 40°



Adapter position for angle-of-attack range from 0° to 20°

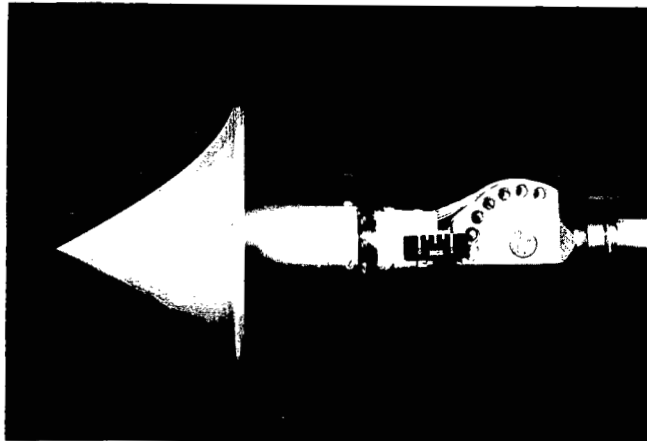
(d) Model on adjustable angle-of-attack adapter.

Figure 2.- Concluded.



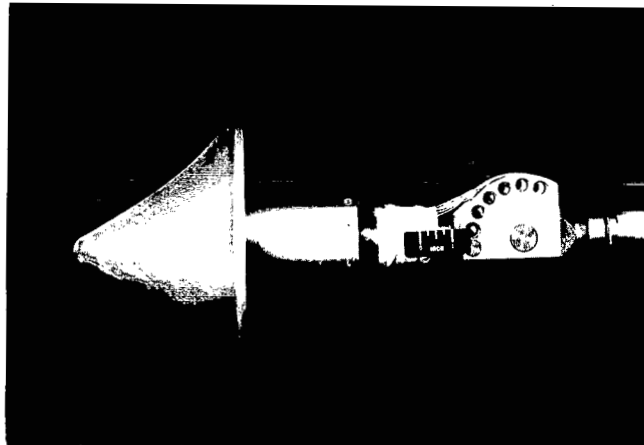
100° conical body with  $r_n/r_b=0.10$

L-65-4903



Tension shell with  $A^2=1.40$  and  $r_n/r_b=0$

L-65-4901



Tension shell with  $A^2=1.40$  and  $r_n/r_b=0.10$

Figure 3.- Photographs of entry models.

L-65-4902

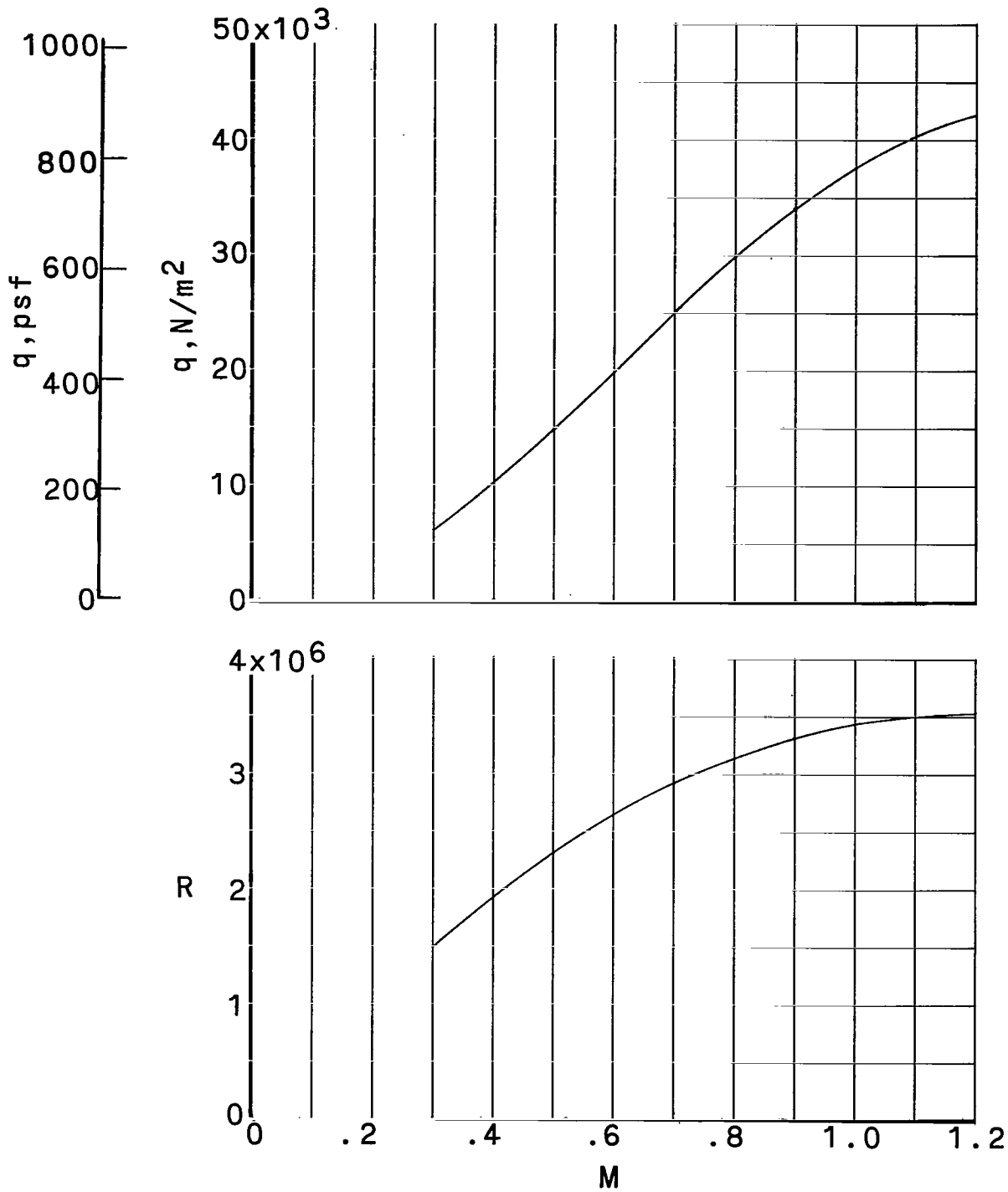


Figure 4.- Variation with Mach number of test dynamic pressure and of test Reynolds number based on reference base diameter  $d = 25.40$  cm (10.00 in.).

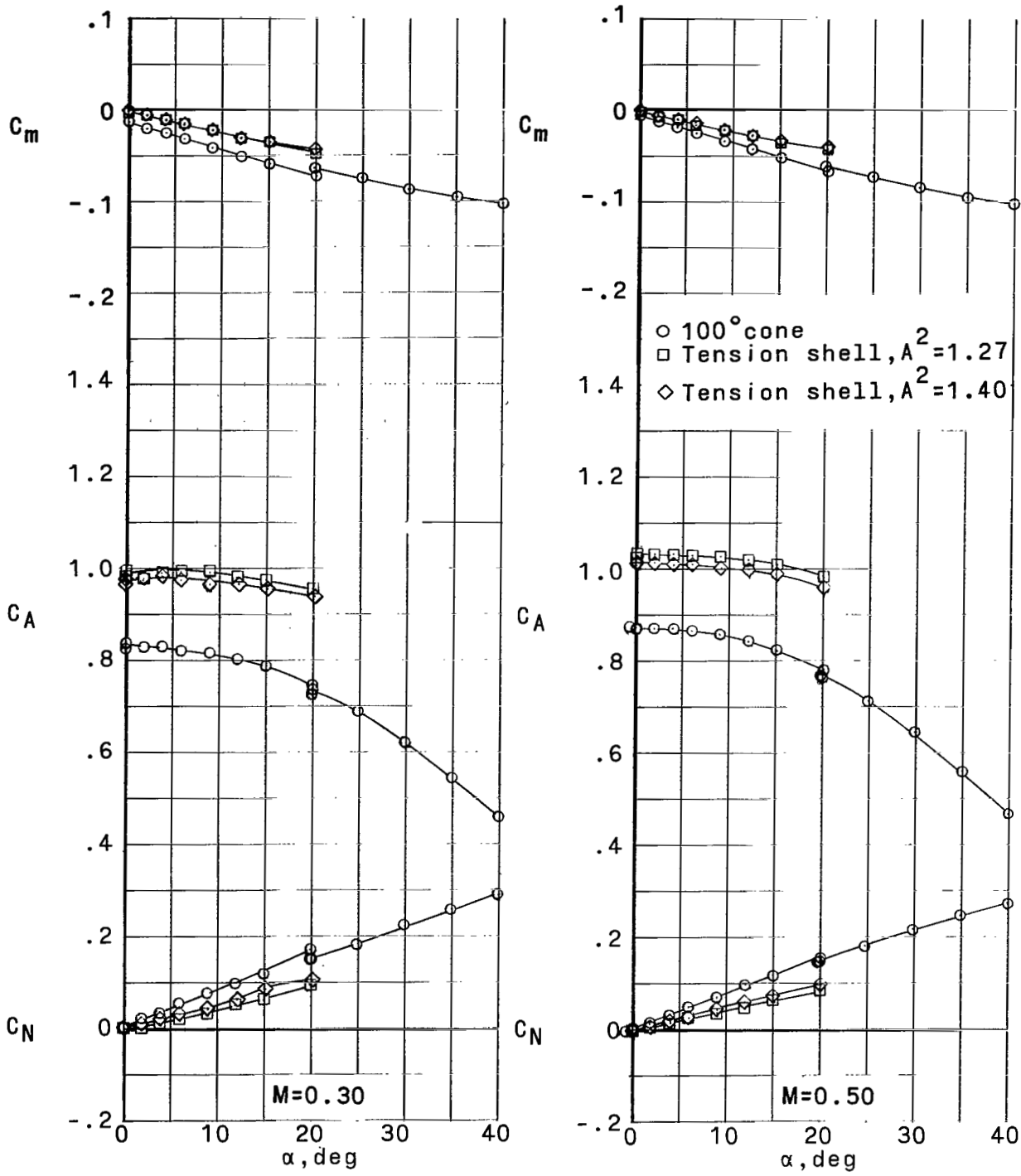


Figure 5.- Variation of longitudinal aerodynamic characteristics with angle of attack for various configurations.  $r_n/r_b = 0.10$ .

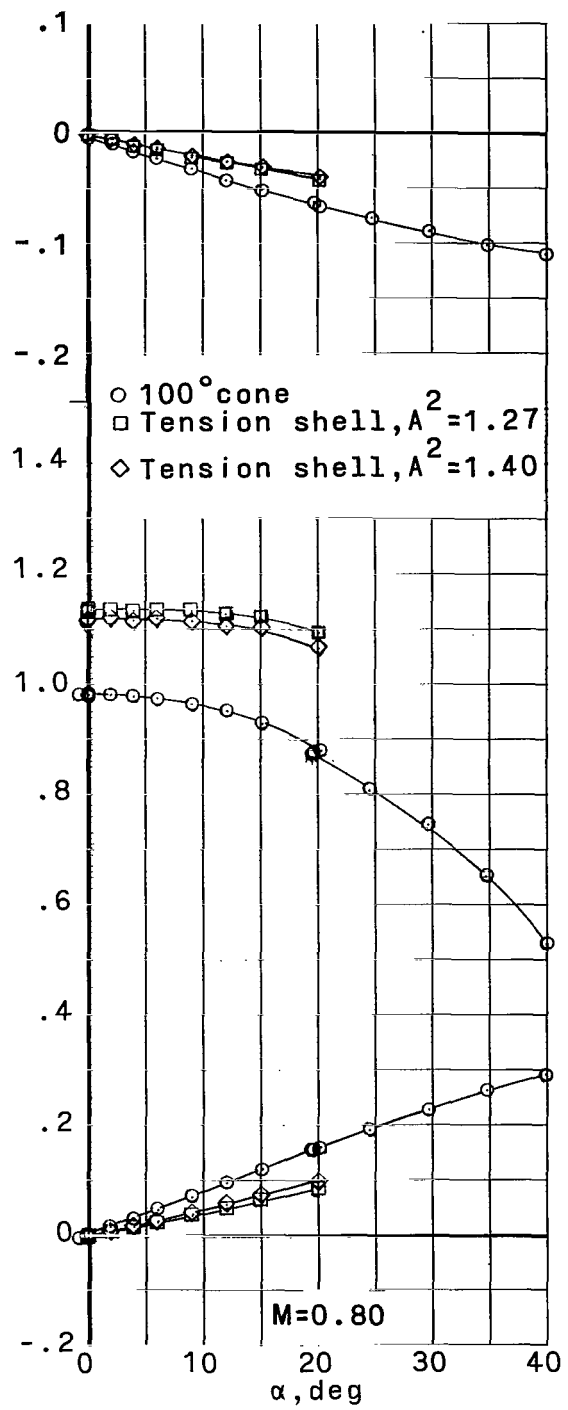
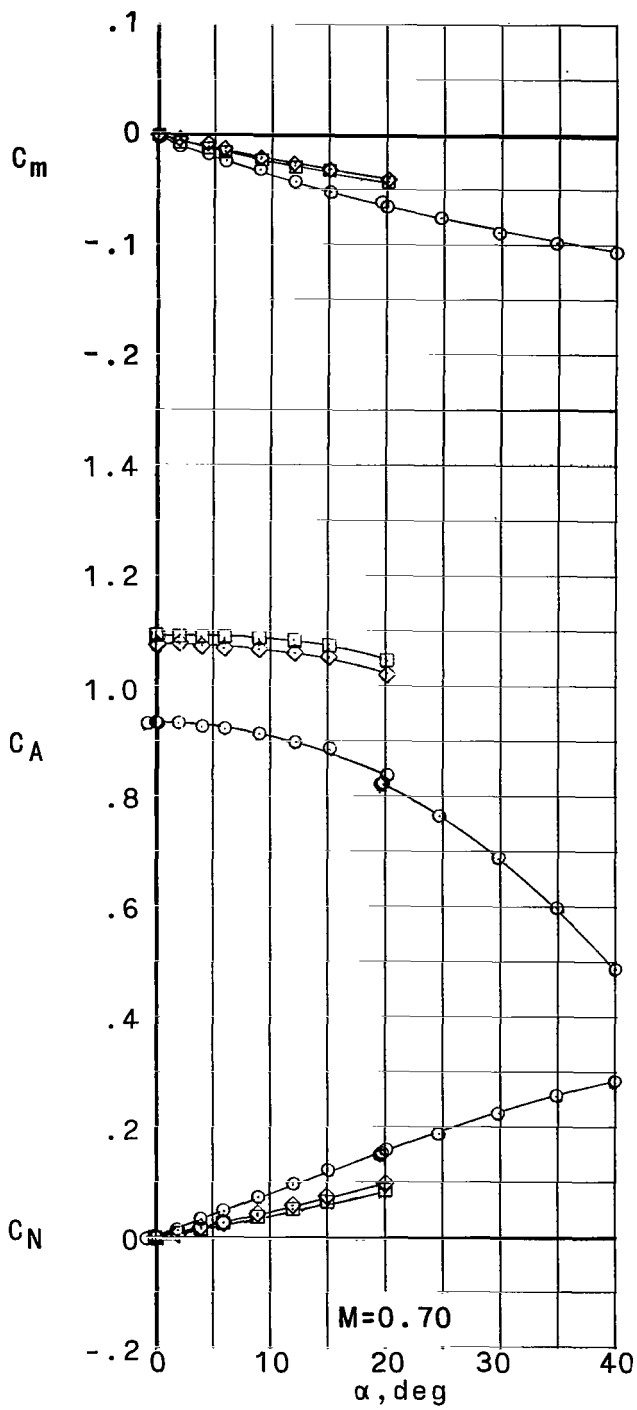


Figure 5.- Continued.

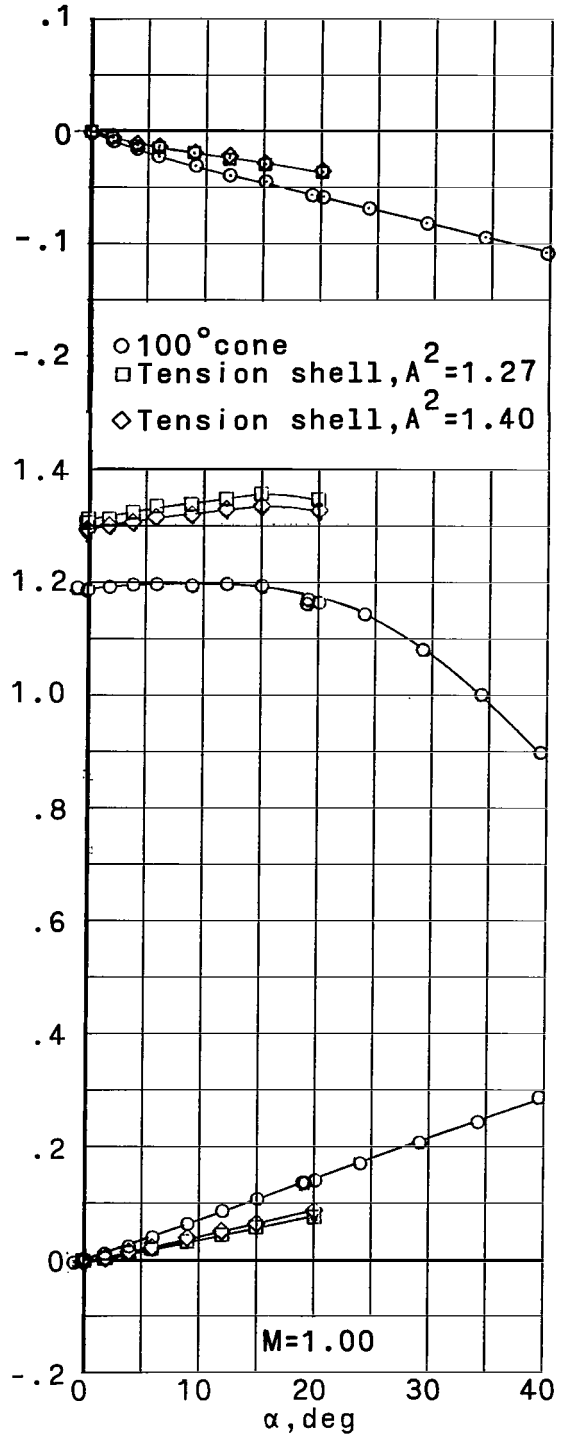
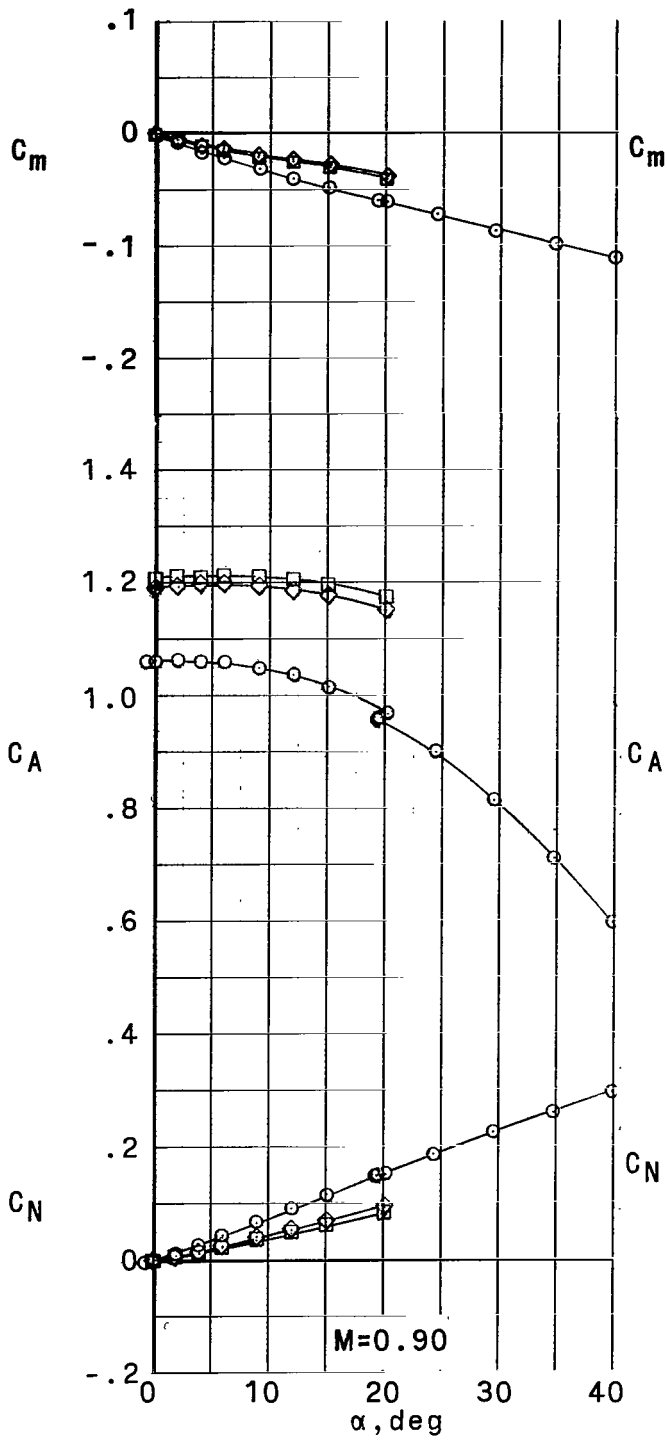


Figure 5.- Continued.

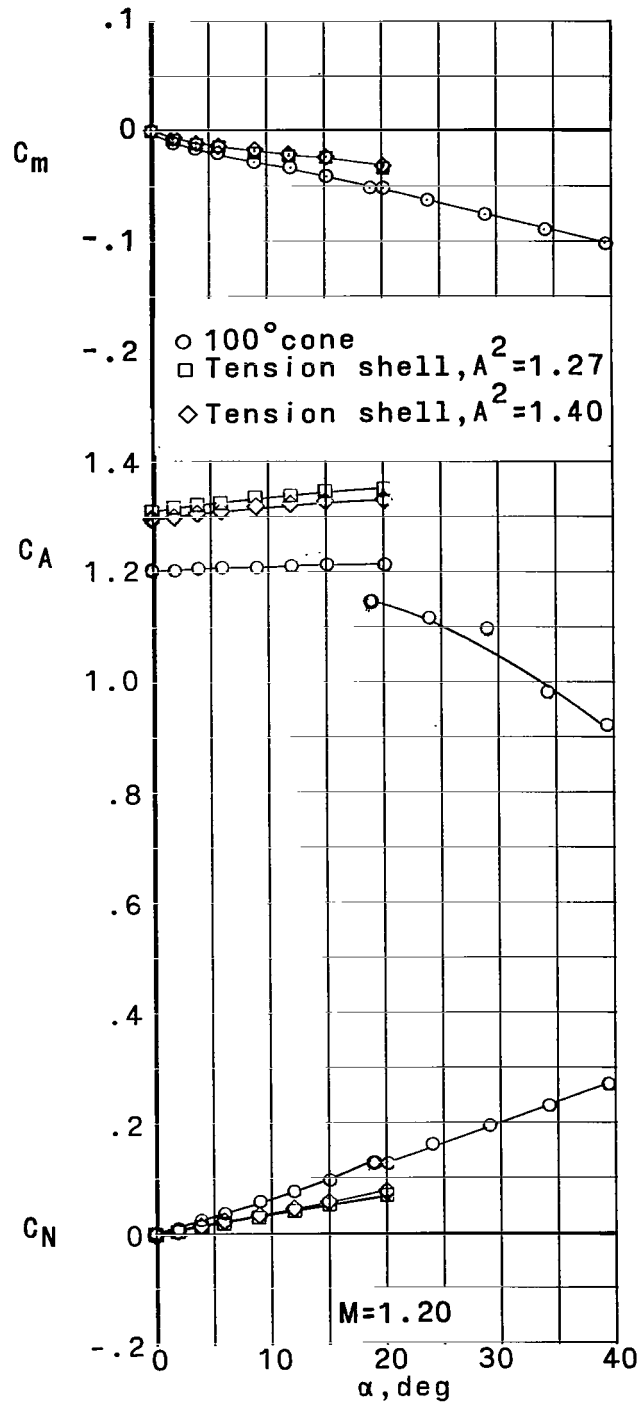


Figure 5.- Concluded.

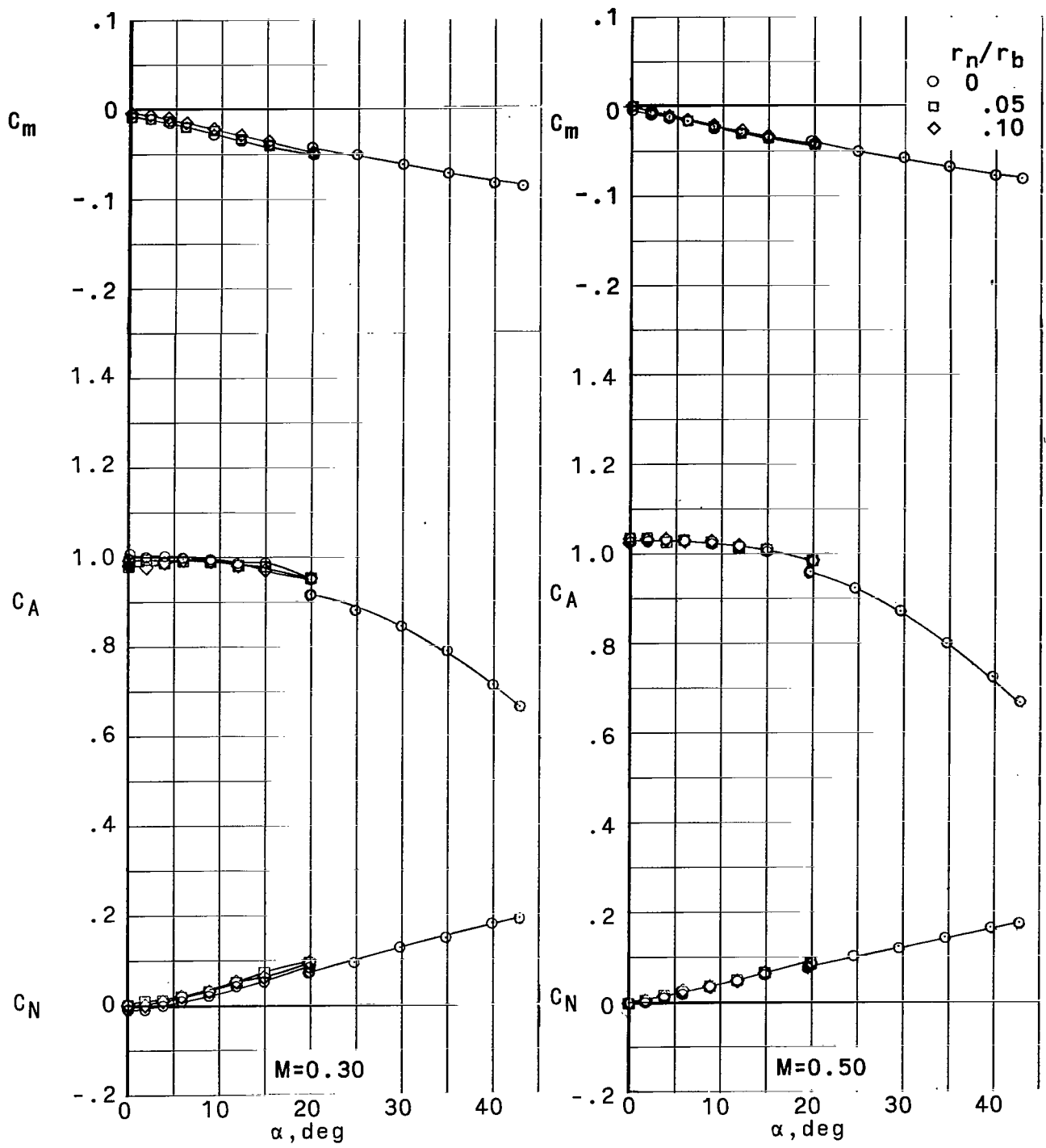


Figure 6.- Effect of nose-bluntness ratio on longitudinal aerodynamic characteristics of tension shell with  $A^2 = 1.27$ .

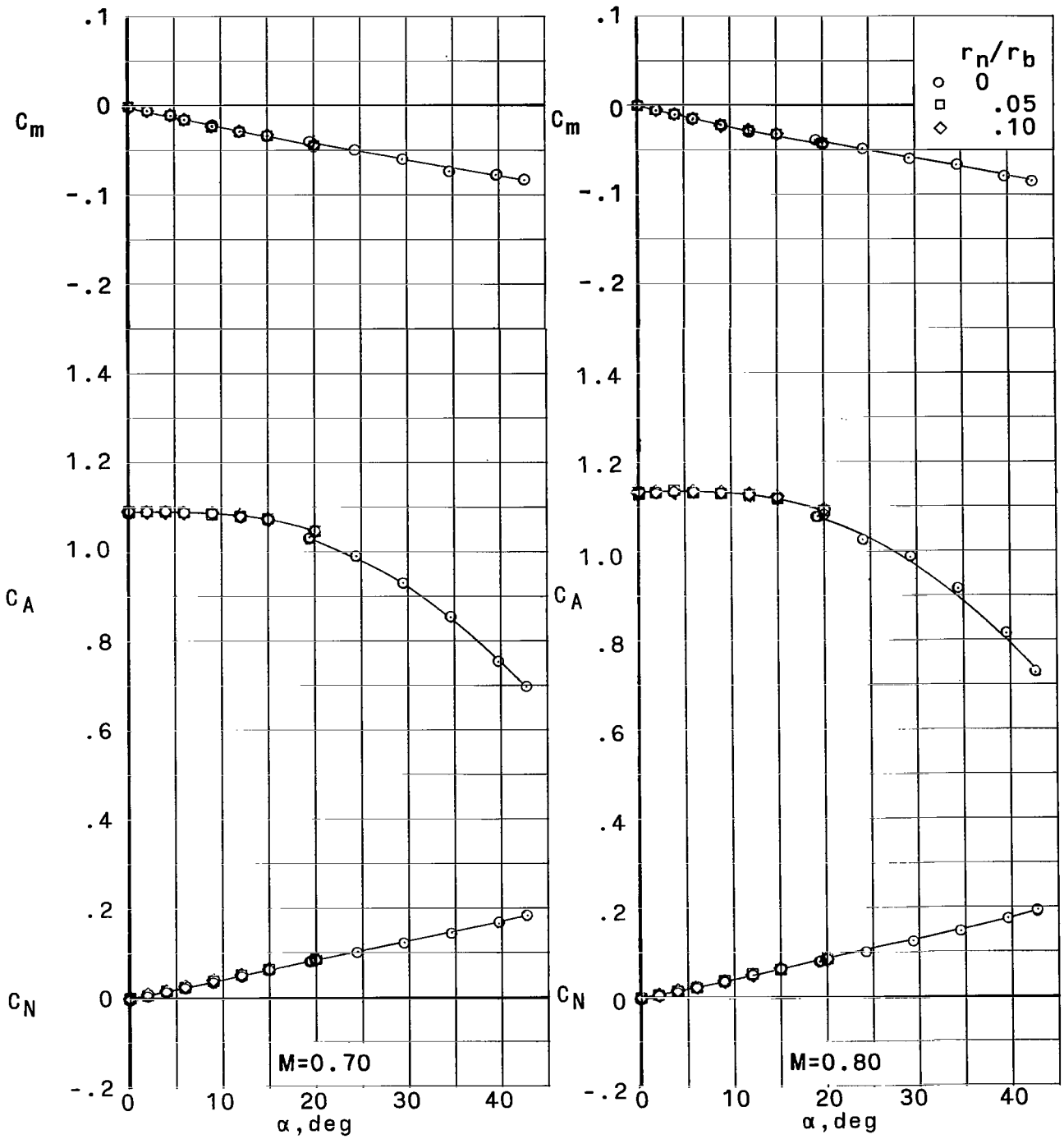


Figure 6.- Continued.

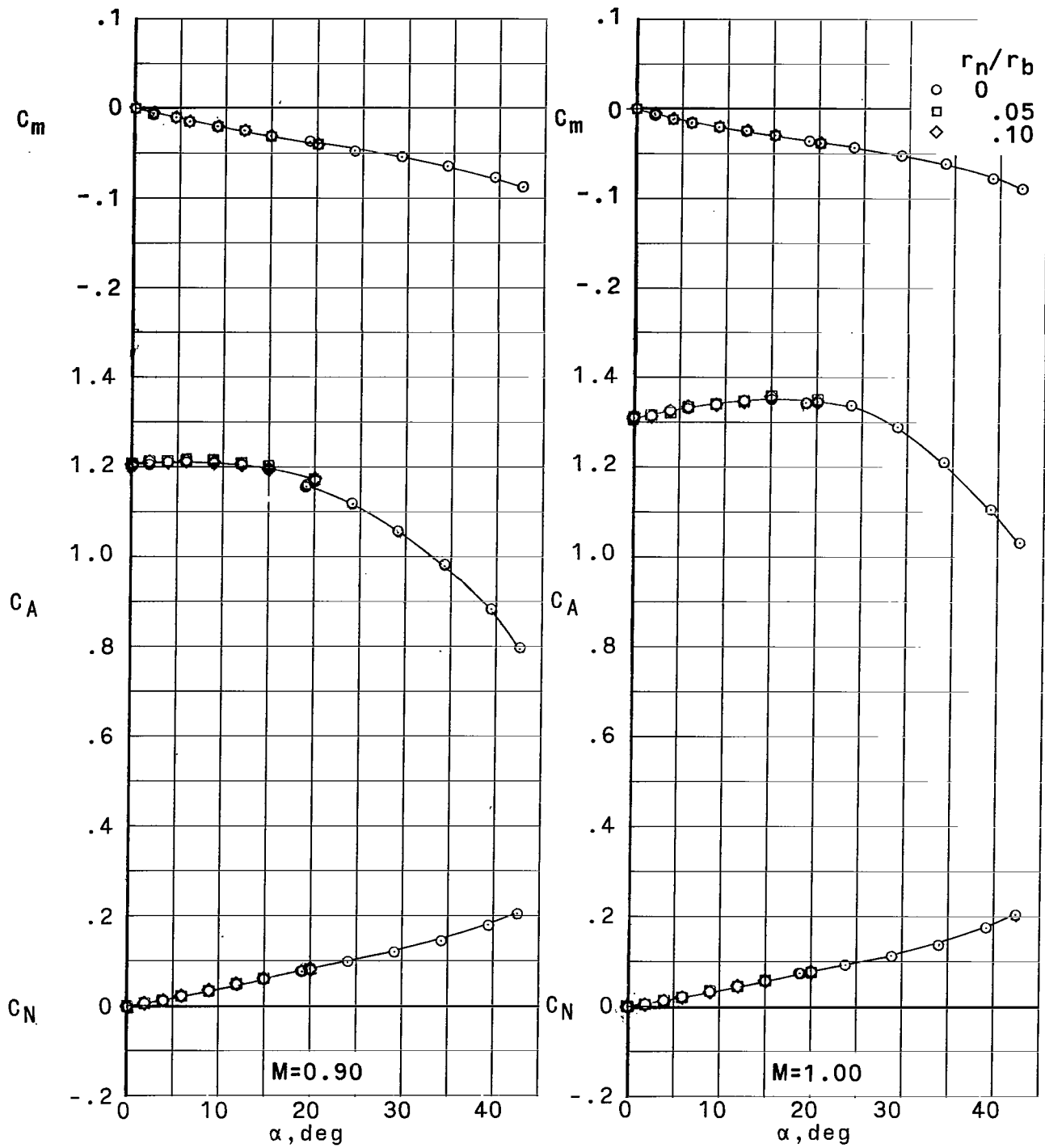


Figure 6.- Continued.

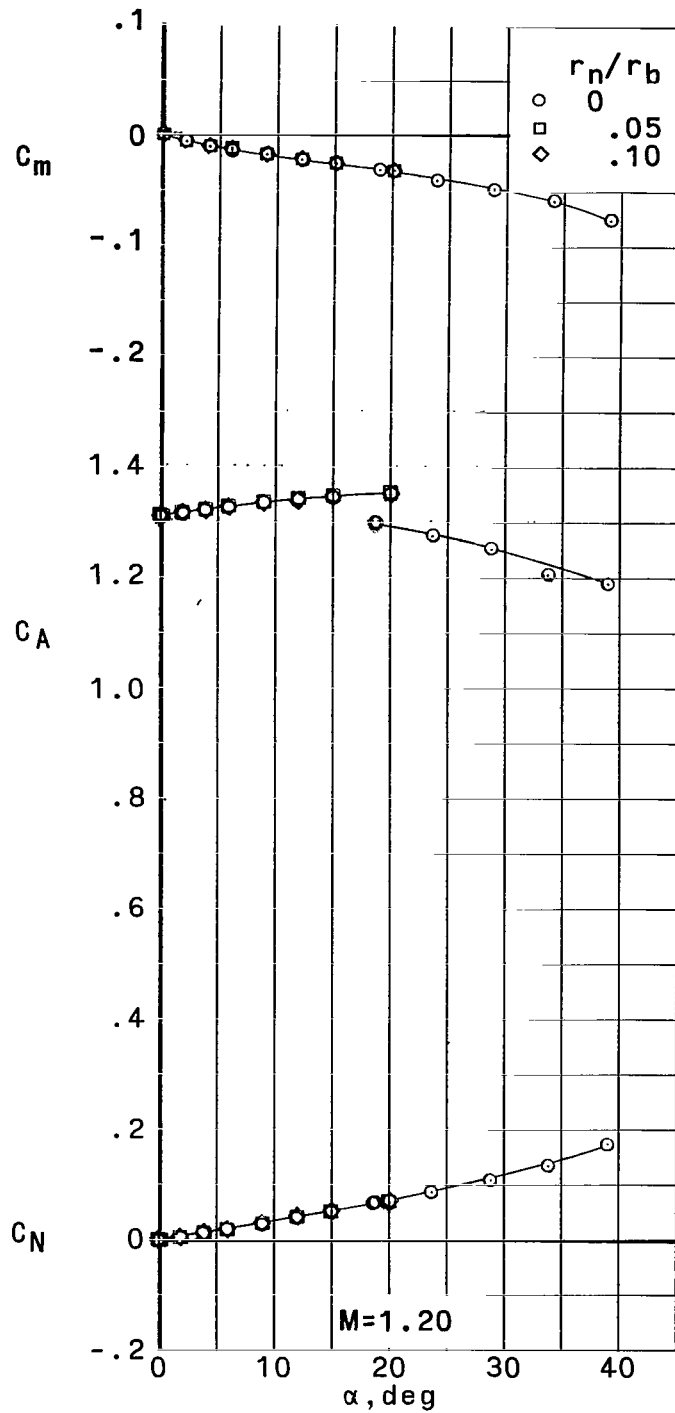


Figure 6.- Concluded.

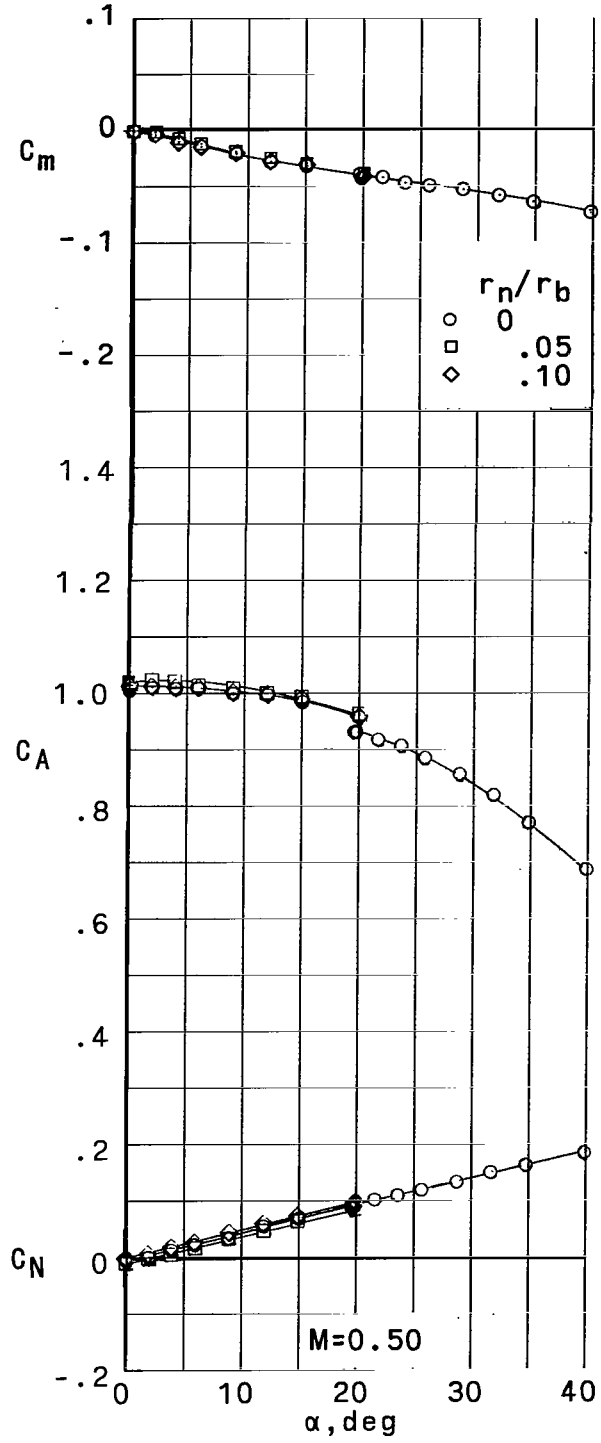
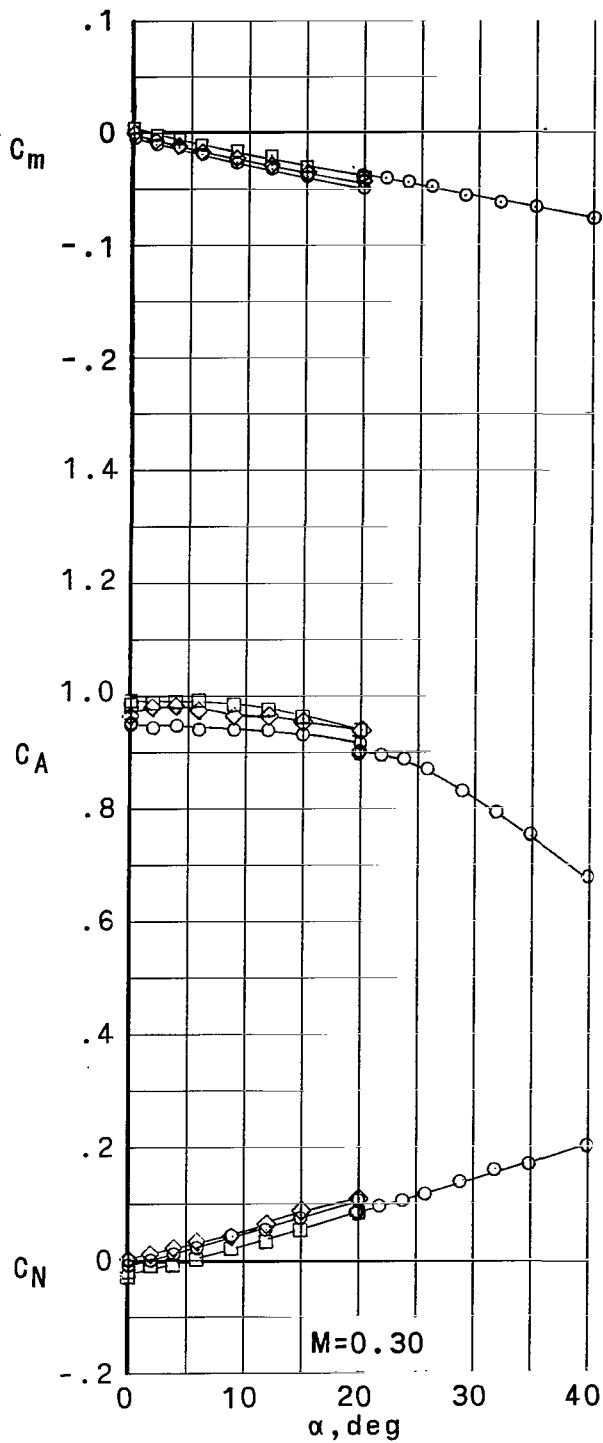


Figure 7.- Effect of nose-bluntness ratio on longitudinal aerodynamic characteristics of tension shell with  $A^2 = 1.40$ .

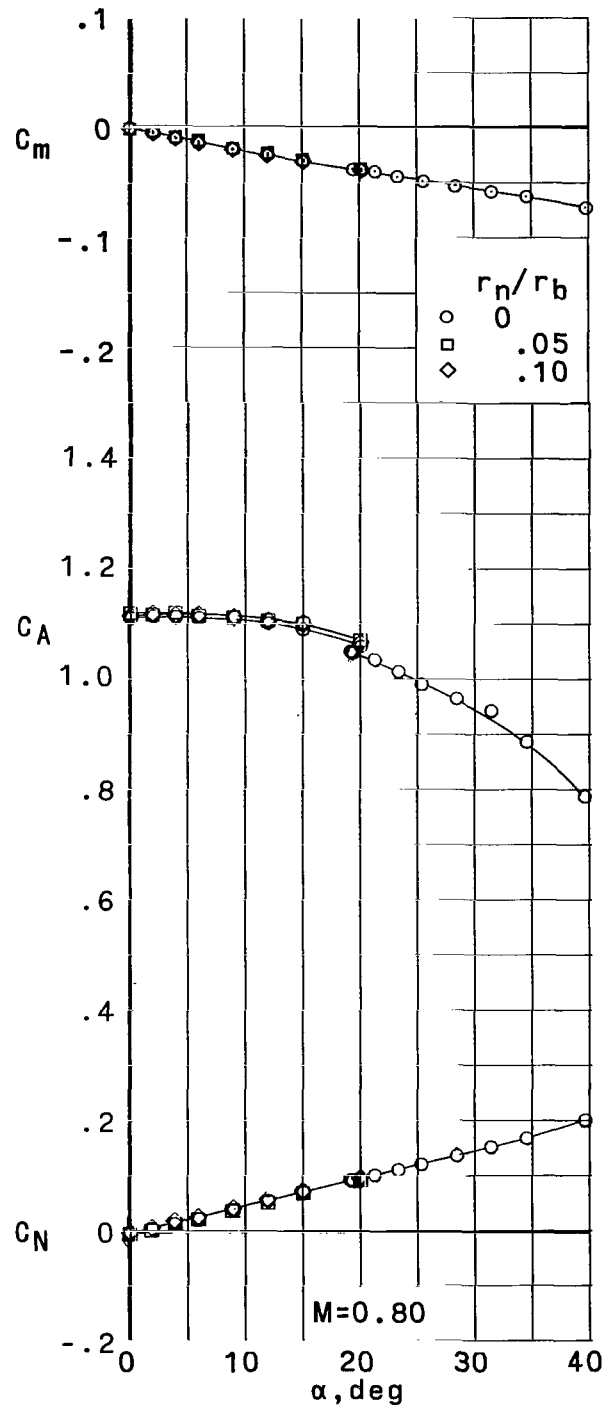
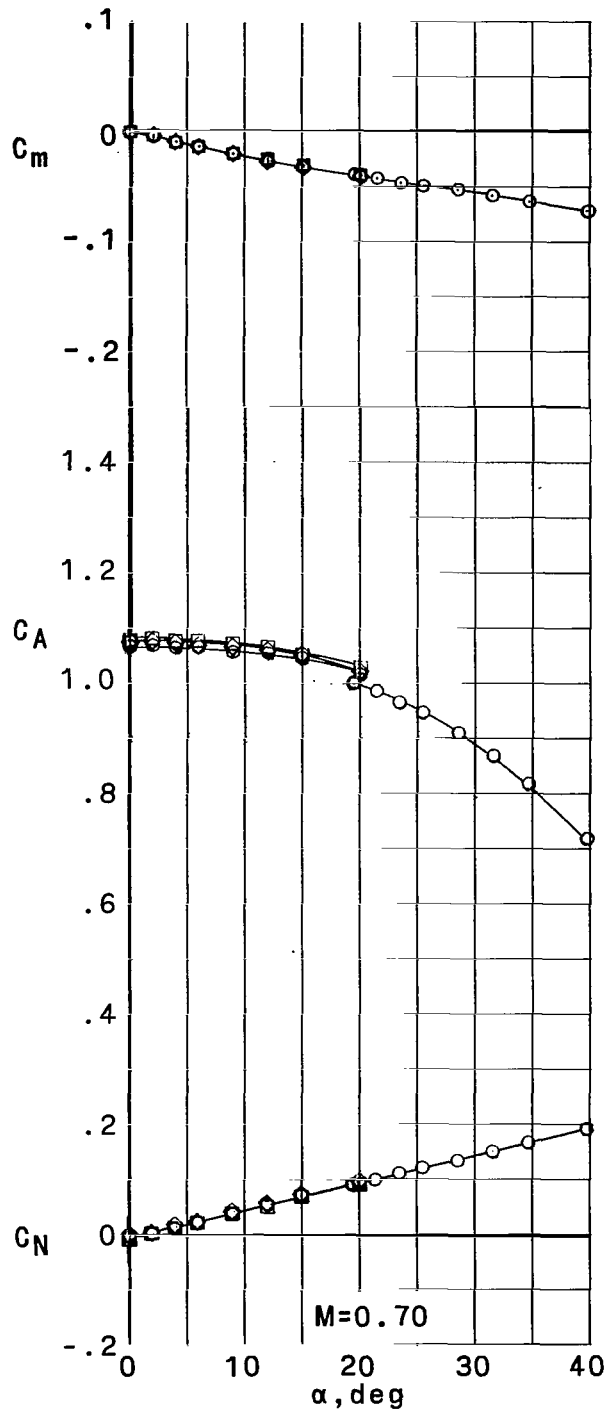


Figure 7.- Continued.

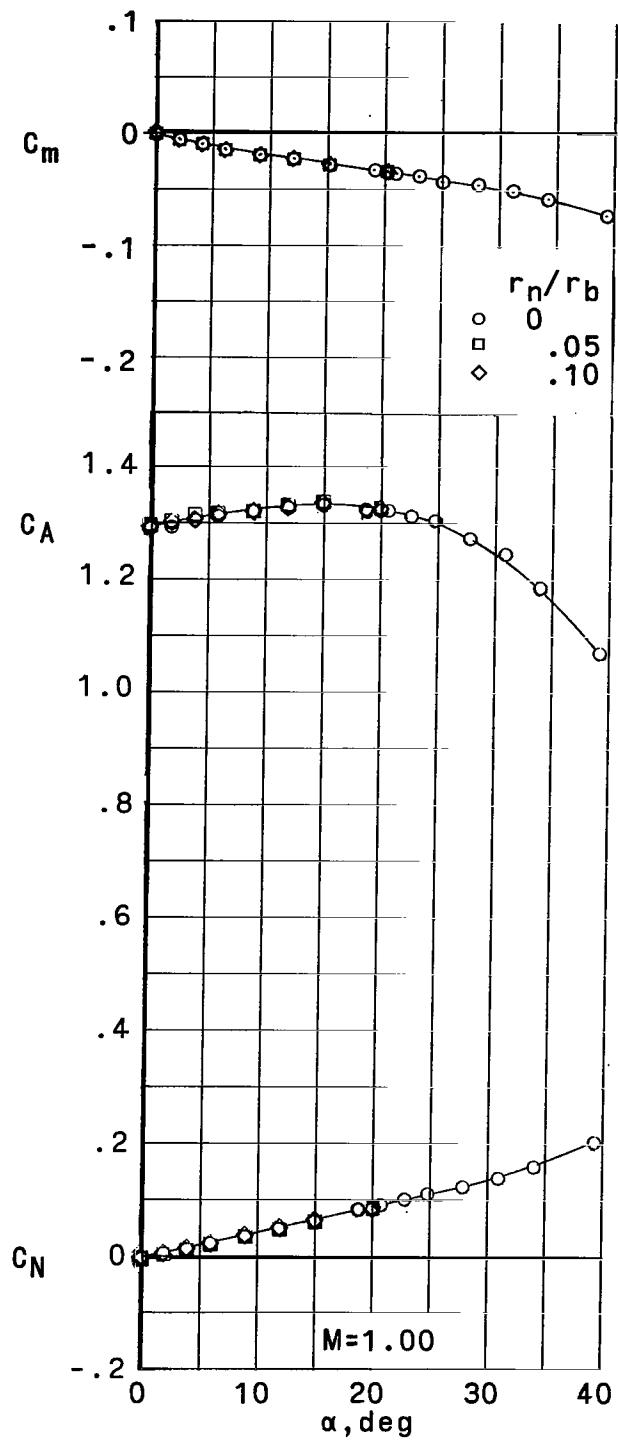
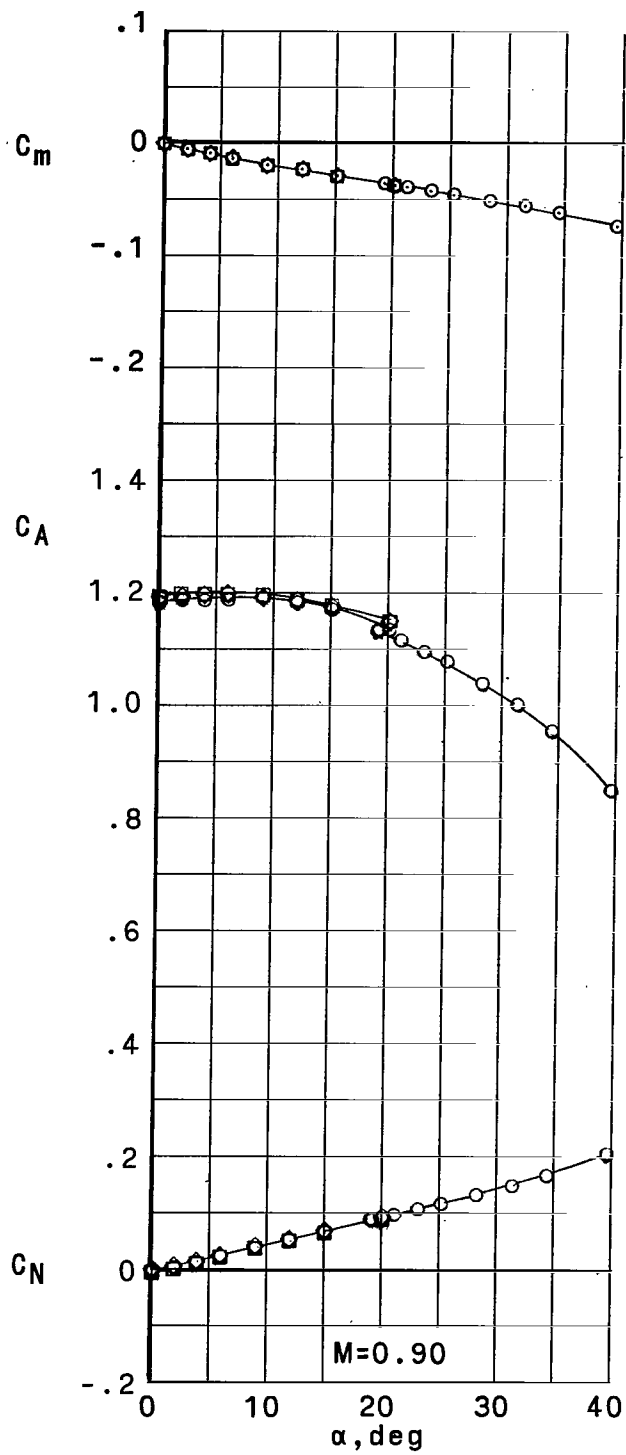


Figure 7.- Continued.

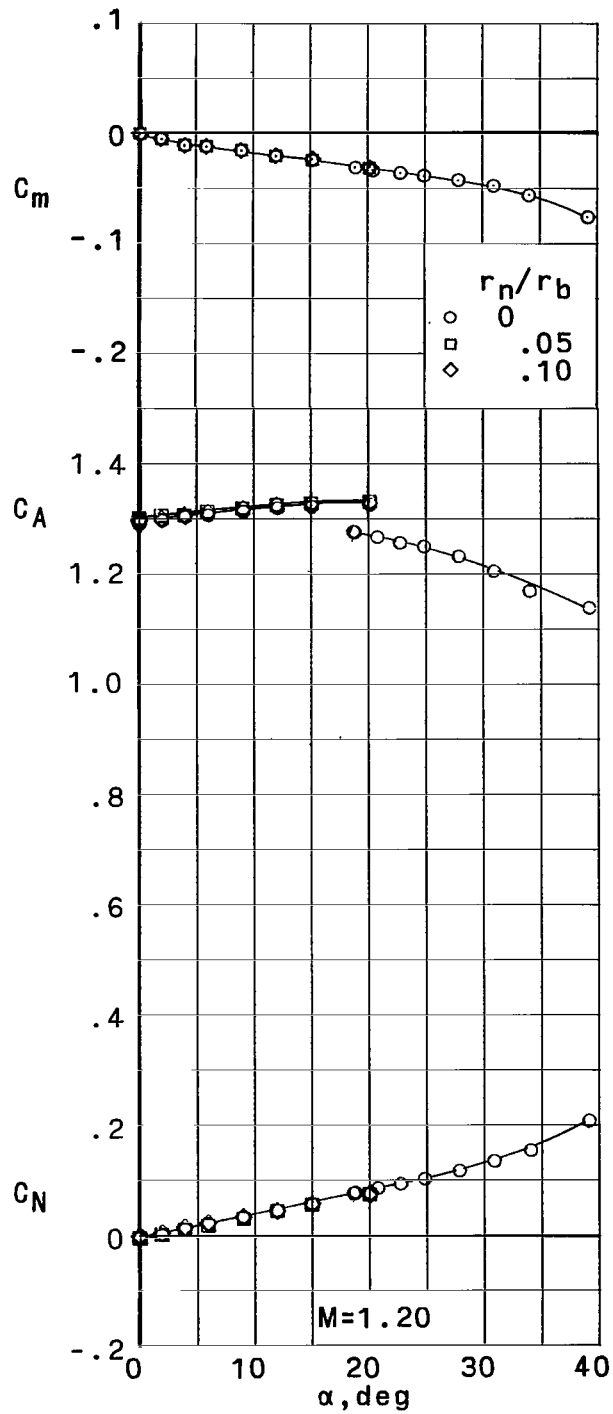


Figure 7.- Concluded.

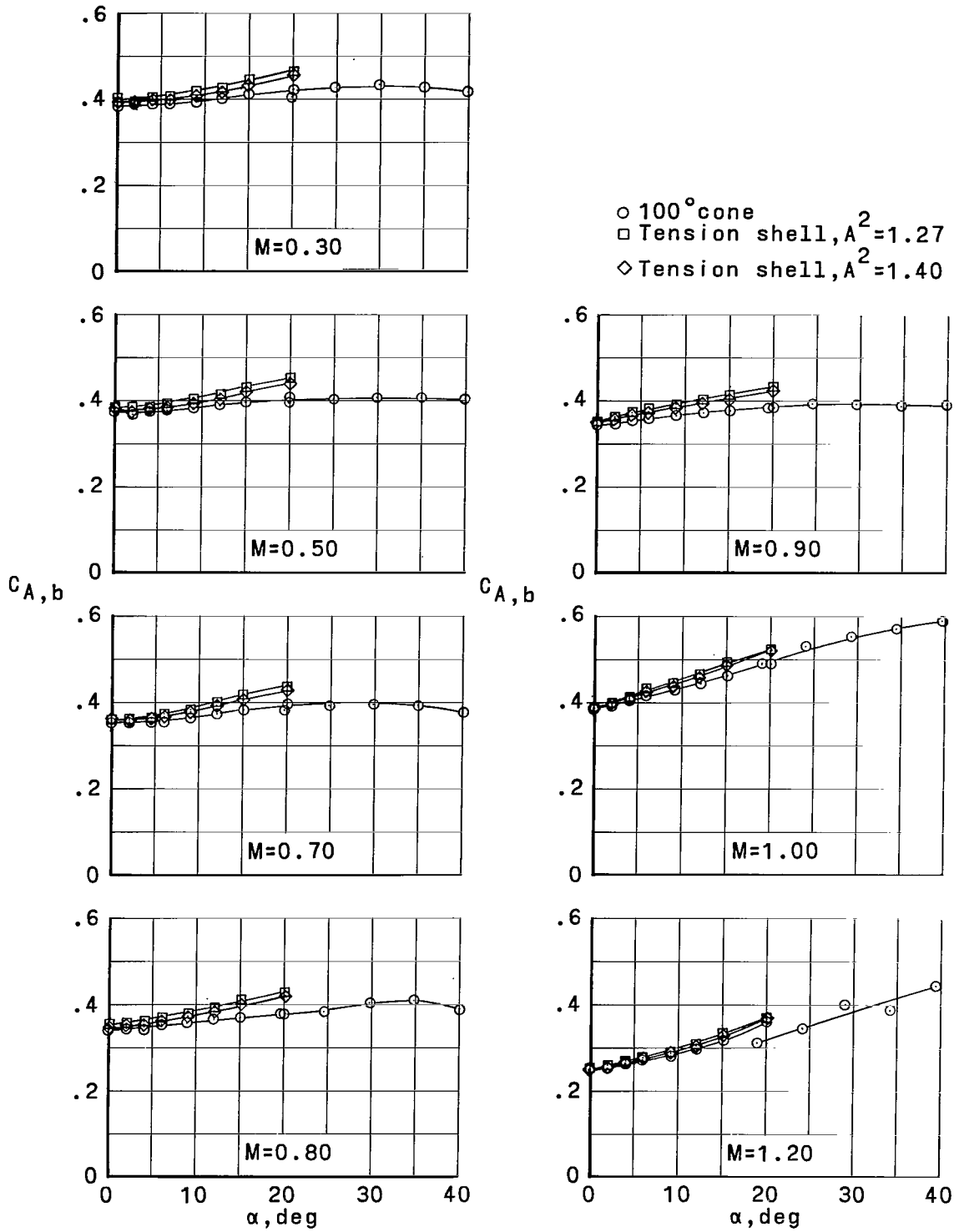


Figure 8.- Representative base axial-force coefficients for various configurations.  $r_n/r_b = 0.10$ .

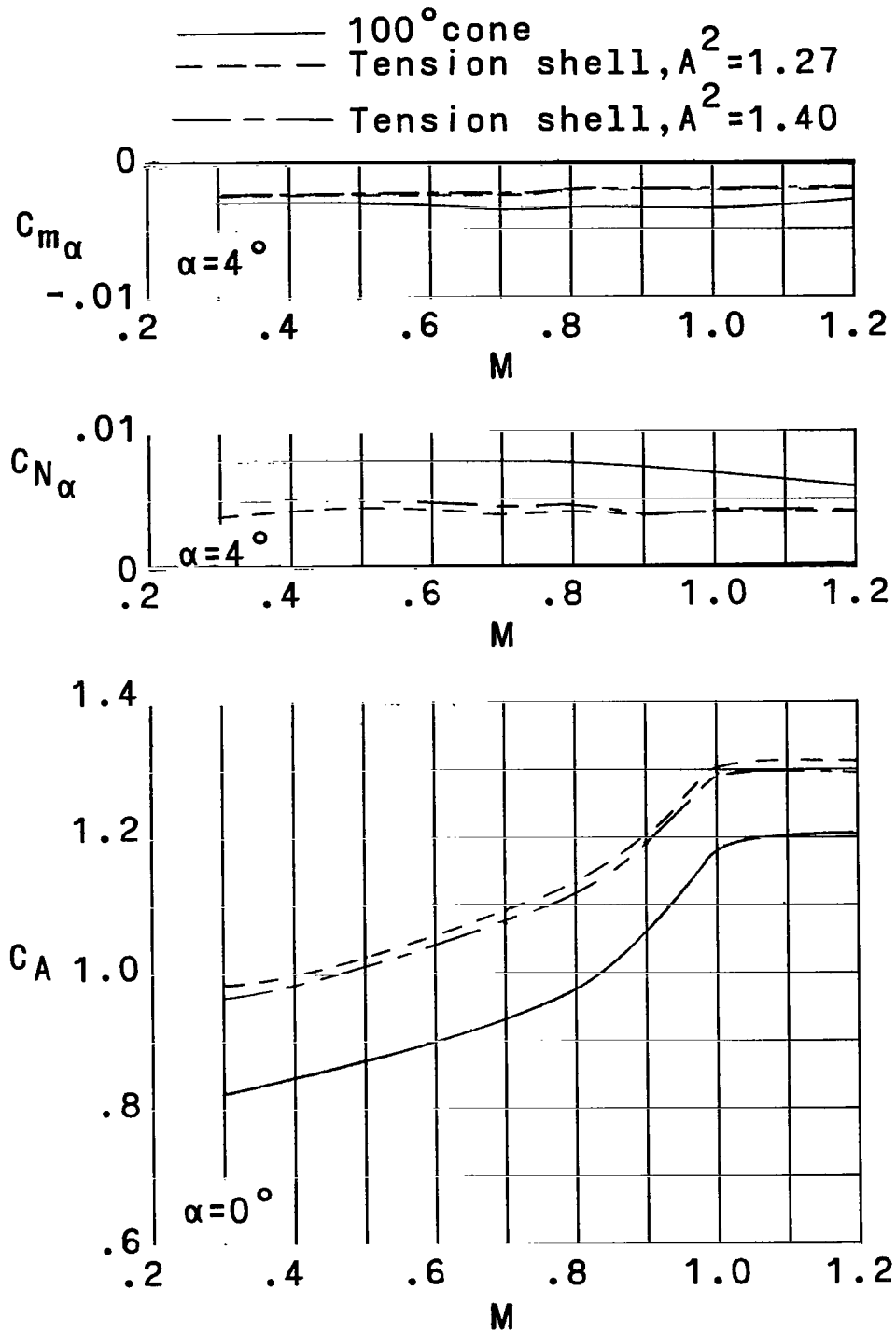


Figure 9.- Variation of  $C_{m\alpha}$ ,  $C_{N\alpha}$  and  $C_A$  with Mach number.

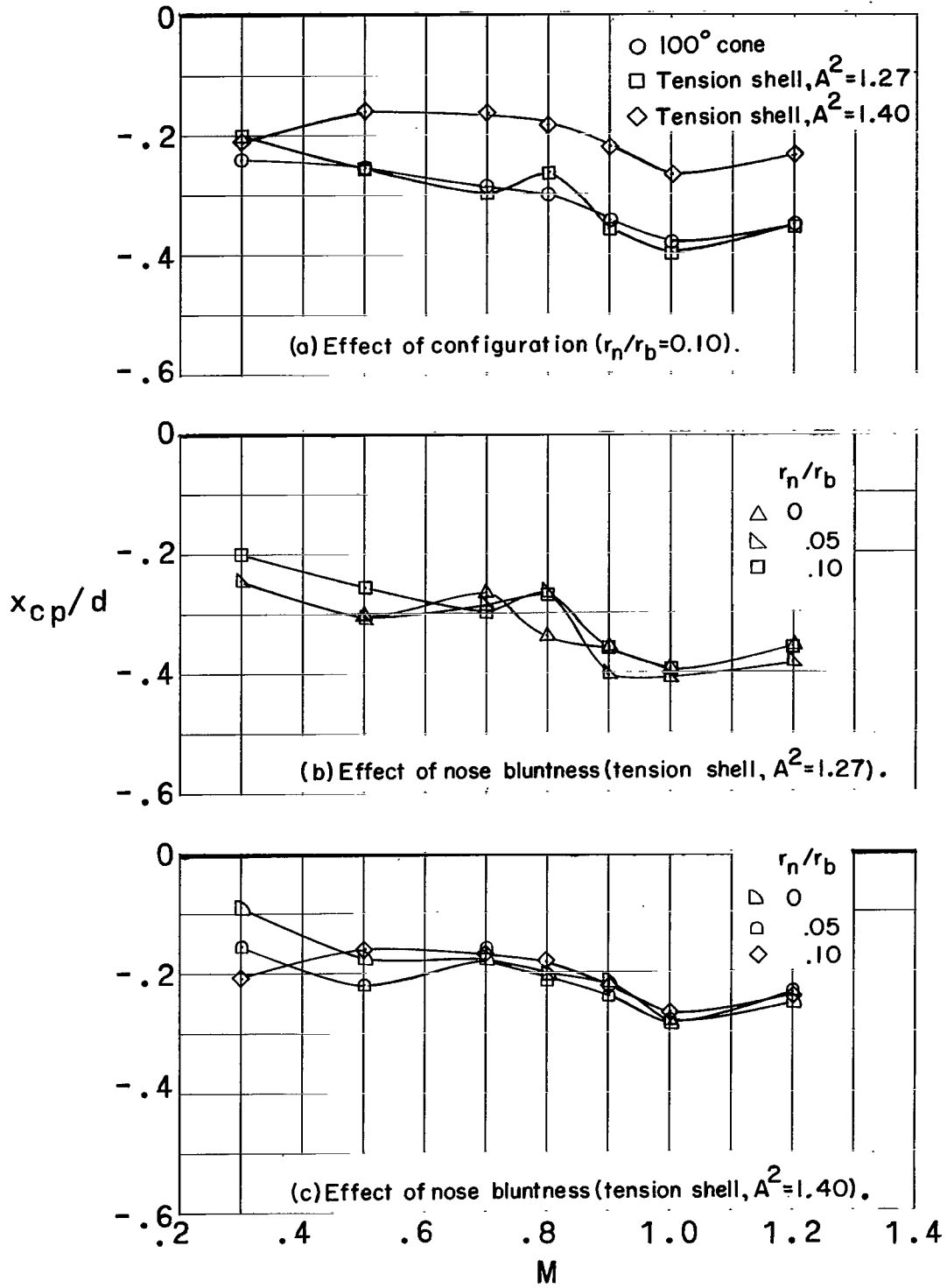


Figure 10.- Variation of center-of-pressure location with Mach number for an angle of attack of approximately  $4^\circ$ .

*"The aeronautical and space activities of the United States shall be conducted so as to contribute . . . to the expansion of human knowledge of phenomena in the atmosphere and space. The Administration shall provide for the widest practicable and appropriate dissemination of information concerning its activities and the results thereof."*

—NATIONAL AERONAUTICS AND SPACE ACT OF 1958

## NASA SCIENTIFIC AND TECHNICAL PUBLICATIONS

**TECHNICAL REPORTS:** Scientific and technical information considered important, complete, and a lasting contribution to existing knowledge.

**TECHNICAL NOTES:** Information less broad in scope but nevertheless of importance as a contribution to existing knowledge.

**TECHNICAL MEMORANDUMS:** Information receiving limited distribution because of preliminary data, security classification, or other reasons.

**CONTRACTOR REPORTS:** Technical information generated in connection with a NASA contract or grant and released under NASA auspices.

**TECHNICAL TRANSLATIONS:** Information published in a foreign language considered to merit NASA distribution in English.

**TECHNICAL REPRINTS:** Information derived from NASA activities and initially published in the form of journal articles.

**SPECIAL PUBLICATIONS:** Information derived from or of value to NASA activities but not necessarily reporting the results of individual NASA-programmed scientific efforts. Publications include conference proceedings, monographs, data compilations, handbooks, sourcebooks, and special bibliographies.

*Details on the availability of these publications may be obtained from:*

SCIENTIFIC AND TECHNICAL INFORMATION DIVISION  
NATIONAL AERONAUTICS AND SPACE ADMINISTRATION

Washington, D.C. 20546